Structural analysis of a dipole system in two-dimensional channels

Ramin Haghgooie and Patrick S. Doyle*

Department of Chemical Engineering and Institute for Soldier Nanotechnologies, Massachusetts Institute of Technology, Cambridge, Massachusetts 02139, USA

(Received 1 July 2004; published 17 December 2004)

A system of magnetic dipoles in two-dimensional (2D) channels was studied using Brownian dynamics simulations. The dipoles interact with a purely repulsive r^{-3} potential and are confined by two hard walls in one of the dimensions. Solid crystals were annealed in the 2D channels and the structural properties of the crystals were investigated. The long-ranged nature of the purely repulsive dipoles combined with the presence of hard walls led to structural deviations from the unbounded (infinite) 2D dipolar crystal. The structures in the channels were characterized by a high density of particles along the walls. The particles along the wall became increasingly localized as the channel width was increased. The spacing of the walls was important in determining the properties of the structures formed in the channel. Small changes in the width of the channel induced significant structural changes in the crystal. These structural changes were manifested in the density profiles, defect concentrations, and local bond-orientation order of the system. Oscillations in the structural properties were observed as the channel width was increased, indicating the existence of magic-number channel widths for this system. As the channel width was increased the properties of the confined system approached those of the unbounded system surprisingly slowly.

I. INTRODUCTION

Magnetorheological (MR) fluids are suspensions of colloids which acquire dipole moments under application of a magnetic field. Traditionally these colloids have been used in macroscopic applications such as controllable dampers, where the ability to tune their bulk rheological properties with a magnetic field has been exploited. Doyle *et al.* [1] have recently shown that the microstructure formed by the colloids in thin gaps can be used to efficiently separate DNA in microfluidic devices. Further fundamental understanding of the self-assembly in confined geometries will allow for greater control of the porosity of colloidal matrices used for biomolecule separations in microfluidic devices. Additionally, it will lead to design principles for many other applications such as field responsive fabrics [2]. Here we investigate the self-assembly of MR fluids in two-dimensional (2D) channels using Brownian dynamics simulations.

Many authors have examined the 2D self-assembly of field-responsive colloids [3–6]. Most of the work has focused on the solid-liquid phase transition in the unbounded system (an infinite 2D system) to try and determine if the melting process is first order as in 3D systems or second order as predicted by theory [7–9]. Others have studied the 2D field-responsive colloid system under various confinements. Most of this research has focused on circular confinements [10–14] and confinement due to a periodic 1D potential [15]. The overriding theme of these studies is that the confinement induces a change in the structural and dynamical behavior of the colloidal crystal and the trends depend upon the nature of the confinement. The 2D channel system is of great interest not only because it is, as of yet, unexplored but also because it serves as a model for understanding self-assembly in microchannels. It is fundamentally important to understand how parallel flat walls affect the properties of the 2D dipolar crystal in order to understand structure formation of MR fluids in rectangular channels.

Several experimental studies have been done on colloidal systems in 2D confined by parallel walls [16–18]. In the first study [16], done on a dusty plasma system, the authors observe that the crystal forms layers in the direction parallel to the walls. They observe that the layered structure decays away from the walls in wide channels and that oscillations occur in the width of the density peaks as the channel width is increased. The most important observation in this study is the anisotropic diffusion of the colloids, enhanced in the direction parallel to the walls and constrained in the direction perpendicular to the walls. The system in the dusty plasma study differs in several important ways from the system studied here. The dusty plasma system was not a truly 2D system in that the "colloids" were actually short chains of particles aligned in the direction normal to the plane of observation. These chains interact differently than repulsive dipoles causing significant differences between the behavior of dusty plasma system and the one studied here. The other studies were done on a system of spherical block copolymers confined by parallel walls [17,18]. In these studies, the authors examine the structure and phase behavior of the system as a function of distance from the wall. They find that the walls help to stabilize a solid structure and the structural properties transition to liquidlike behavior as the center of the channel is approached. The channels in this study were three orders of magnitude larger than the block copolymers so the effects of tight confinement were not probed.

A 3D system, similar to the 2D channel, that has been studied in detail is confinement of a liquid film in a narrow slit between two parallel planes. It is well known that liquids confined in a thin gap form layered structures characterized

*Electronic address: pdoyle@mit.edu

by oscillations in the density profile normal to the confining planes [19]. The properties of the density profiles of this system have been shown to depend on the separation of the two confining planes [20]. This bears resemblance to the 2D channel system where the confining walls also impart structure to the confined medium but there are many other rich structural changes induced by the confinement which we will discuss in detail.

The organization of this paper is as follows. In Sec. II we provide details about the simulations performed in this study. In Sec. III we discuss the structural properties of the 2D channel system at zero temperature (when thermal fluctuations are negligible). The structure of the system at a finite (nonzero) temperature is investigated in Sec. IV. The layering of the colloids at this finite temperature is discussed in Sec. IV A and the properties of the layers closest to the walls are further investigated in Sec. IV B. The properties of the crystal in the 2D channel are compared to those of the unbounded crystal in Sec. IV C. The results and impact of this study are summarized in Sec. V.

II. SIMULATION DETAILS

The system studied in the present work contains purely repulsive magnetic dipoles in 2D confined in one lateral direction between two hard walls. The colloids interact with the walls only via hard-sphere interactions. This 2D channel system also serves as a preliminary model for studying the structural properties of the 3D MR fluid structures formed in microfluidic devices. In these devices, the structures are columns of magnetic particles which span the height of the channel and repel each other in the lateral directions. When viewed from the top, the columns can be modeled by a 2D plane containing purely repulsive dipoles. This model fails to capture the effects of chain coalescence that occur in a truly 3D system [21], but it serves as a starting point for understanding the intercolumn structure in the channel system.

The MR colloids confined to a plane are modeled as hard spheres with repulsive point dipoles at their centers when the field is directed normal to the plane of the 2D system. The point-dipole approximation for MR colloids in 2D is very common in the literature [6,22] and has been shown to be a good approximation for the magnetic behavior of MR colloids [23]. It has even been used to generate meaningful results in the case where hard walls are present in the system [11,13]. Additionally the effects of mutual induction between particles in this system are negligible due to the large separation distances between the particles. Therefore, the magnetic interactions in the system are dominated by the large magnitude of the applied external field. The pairwise dipolar interaction energy (V_{ij}) between the colloids is

$$V_{ij}(r_{ij}) = \epsilon \left(\frac{d}{r_{ij}} \right)^3, \quad (1)$$

where $\epsilon = \mu_0 M(B)^2 / 4\pi d^3$ is the energy scale and d is the diameter of the hard sphere. The center-to-center distance

between the two particles i and j is given by r_{ij}, μ_0 is the magnetic permeability of free space, and $M(B)$ is the dipole moment of an individual colloid and is a function of the magnetic field strength (B). A dimensionless field strength is then defined as

$$\Gamma = \frac{\epsilon}{k_B T} \left(\frac{d}{R} \right)^3, \quad (2)$$

where R is the natural length scale for these systems, defined as $R = a \sin 60°$. The parameter a is the lattice spacing in a perfectly hexagonal lattice and the angle $60°$ is the characteristic angle for a hexagonal lattice. The length scale R corresponds to the spacing between two neighboring lattice lines in the hexagonal lattice. A lattice line is a line of particles in the 2D crystal along one of the lattice vectors. The lattice spacing (a) depends on the number density in the system $[a = (n\sqrt{3}/2)^{-1/2}]$ where the number density (n) is defined as the number of particles per unit area ($n = N/A$) and A is defined as the area available to the centers of the particles. Therefore, the length scale is written in terms of the number density as

$$R = \left(\frac{2}{\sqrt{3}} n \right)^{-1/2}. \quad (3)$$

This length scale differs from ones used in previous studies of the 2D dipolar unbounded system [4,24,25] by a constant, but is appropriate for the 2D channel system as discussed in Sec. III. The dimensionless interaction energy in the system is defined as

$$\frac{V_{ij}(r_{ij})}{k_B T} = \Gamma \left(\frac{R}{r_{ij}} \right)^3, \quad (4)$$

and the dimensionless temperature in the system is $1/\Gamma$. Nondimensionalizing the system properties in this way results in the interesting observation that all 2D dipolar systems at the same temperature behave identically, independent of the number density in the system as long as R is the only relevant length scale in the system (i.e., $d \ll R$) as is the case for all of the results reported here.

To study the 2D dipole system we used the Brownian dynamics simulation technique [26]. The equation of motion is approximated by the stochastic differential equation

$$\dot{\mathbf{r}}_i(t) \simeq \frac{1}{\zeta} \mathbf{F}_{s,i}(\mathbf{r}_j(t)) + \sqrt{\frac{2 k_B T}{\zeta \delta t}} d\mathbf{W}_i, \quad (5)$$

where the inertia of the particles is neglected. The parameter $\mathbf{W}_i$ is a Wiener process with $\langle d\mathbf{W}_i \rangle = 0$ and $\langle d\mathbf{W}_i d\mathbf{W}_j \rangle = \delta_{ij} \boldsymbol{\delta}$ and represents the thermal fluctuations. $\mathbf{F}_{s,i}(\mathbf{r}_j(t))$ is the sum of all pairwise interactions in the system including dipole-dipole interactions and ζ is the drag coefficient on a single particle. A simple Euler integration scheme was used for the time integration. At the end of a time step, hard-sphere excluded volume interactions were treated by displacing overlapped particles along the line connecting their centers until they are just contacting each other as discussed in [27]. Particles that overlap with the wall were displaced normal to the wall until they just contacted the wall. This procedure was

performed in a pairwise fashion and was iterated until all overlaps were removed and then the simulation proceeded to the next time step. In the case of our 2D dipolar system there were never particle-particle overlaps, only particle-wall overlaps, because the repulsive potential between particles is so large for the field strengths used in our study.

For the simulations of the unbounded system, periodic boundary conditions were imposed in both the x and y directions and the number of particles was 14 784. The simulations of the channel system had periodic boundary conditions in the y direction and hard-wall boundaries in the x direction. The number of particles varied from 960 to 3840. Hydrodynamic interactions were neglected for simplicity as they do not affect the structural properties of the 2D crystal and they are screened in thin gaps. A time step $\delta\tilde{t}$ of 7.5×10^{-5} was employed where time is made dimensionless as $\tilde{t} = t k_B T / \zeta R^2$. The value $\zeta R^2 / k_B T$ is approximately the time necessary for a particle to freely diffuse a unit length R. A cutoff of $6.5R$ was used for the dipole-dipole interactions in conjunction with a linked-list binning algorithm [28] using bin sizes slightly larger than the cutoff for the dipole-dipole interactions. Only interactions with particles closer than the cutoff were considered. All of the simulations reported here were done holding number density constant at $n = 0.0462$ and were confirmed to be converged in system size, time step, and cutoff. In the channel systems, the width of the channel is taken to be the space which the center of a particle can access and therefore the area used in calculating the number density is the true area minus two area elements $d/2$ wide, one at each wall. In defining the channel width in this manner, we remove any system dependence on d for $d \ll R$. In the unbounded systems, the area is simply the true area. The systems were equilibrated for $\tilde{t} = 373$ and statistics were taken for $\tilde{t} = 37.3$. Taking statistics over a longer period of time did not change the results and therefore was considered unnecessary.

The 2D unbounded system was carefully simulated using 14 784 particles in order to determine the dimensionless temperature at which the system transitions from a solid to a liquid. It was determined that above a dimensionless temperature of 0.0672 the 2D unbounded system is a liquid and below a dimensionless temperature of 0.0658 it is a solid, in agreement with the literature [3]. Between these two temperatures, we were unable to converge the simulations because of the diverging correlation lengths that occur near the phase transition [29].

III. ZERO-TEMPERATURE-ANNEALED STRUCTURES

The 2D channel system was annealed from an equilibrated liquid state to a very low temperature ($1/\Gamma = 0.02$). The channel system is found to be in the solid phase at this temperature. The annealing process was performed at varying rates and with sequential heating and cooling to ensure an equilibrium structure at a temperature of 0.02. The system was then quenched to zero temperature by setting the stochastic term in Eq. (5) to zero. This turns off the Brownian motion, effectively causing $1/\Gamma$ to go to zero. This quenching was done from a variety of different starting configura-

(a)

(b)
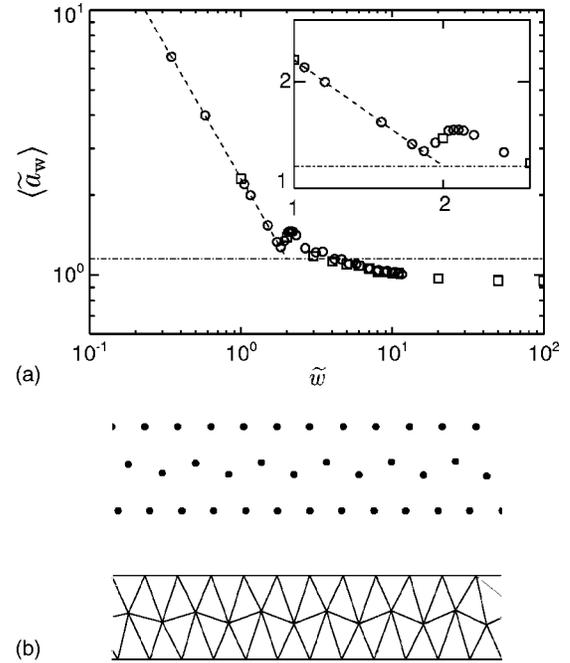
FIG. 1. (a) The average dimensionless wall spacing for different dimensionless channel widths; square symbols correspond to integer channel widths and circle symbols correspond to noninteger channel widths. The dash-dotted line corresponds to the dimensionless 2D unbounded lattice spacing and the dashed line corresponds to the dimensionless 1D lattice spacing. The oscillations in wall spacing as a function of channel width are continuous (inset). (b) The crystal aligns with the channel walls (top) and remains hexagonal in the Delaunay triangulation (bottom) for a dimensionless channel width of 3.

tions within the equilibrated crystal. The final internal energy of all the quenched systems for a given channel width did not vary by more than 1%.

The zero-temperature crystal was observed to align with one of its lattice vectors along the length of the channel, parallel to the confining walls as seen in the top of Fig. 1(b). From this observation we note that there should be certain channel widths, magic numbers, that are fully commensurate with the natural spacing of an unbounded crystal aligned in the direction parallel to the walls. We will show, however, that these magic numbers are not simply integer multiples of R, as implied by the alignment of the crystal, but are affected by a number of the properties of the 2D crystal in channels. A structural characteristic of the zero-temperature structures in channels is the dimensionless wall spacing $\tilde{a}_w$ which is defined as the distance between adjacent particles along the walls. In Fig. 1(a) the dimensionless wall spacing is seen to follow exactly the 1D lattice spacing for channel widths less than ~ 2. The 1D lattice spacing [dashed line in Fig. 1(a)] is the calculated wall spacing for a constant n channel system in which the particles are aligned in two rows, one at each wall. In the large channel limit the wall spacing approaches a constant, showing the behavior of a semi-infinite system. The value that is approached ($\sim 0.83a$) is actually less than the spacing of the 2D unbounded crystal meaning that the line density of the lattice line on the wall is larger than that of a

lattice line in the unbounded 2D crystal. The line density is defined as the number of particles per unit length along a lattice line and is a constant equal to a^{-1} along the lattice lines of an unbounded 2D lattice. The increased line density along the wall is explained by noting that the walls remove some of the energetic penalty associated with a higher line density. In the unbounded 2D crystal, increasing the line density of a row in the crystal results in a higher interaction energy between the particles in that row (i.e., the spacing between particles in the row is reduced) and a higher interaction energy between that row and adjacent rows. In the channel system, the row of particles at the wall has only one neighboring row, not two, so the energetic penalty for increasing the line density along the wall is lower than for the unbounded 2D crystal. The consequences of the higher density of particles along the wall will be discussed further in Sec. IV A.

In Fig. 1(a) there is a nonmonotonic decrease in the wall spacing characterized by a series of decaying oscillations as the channel width is increased. The largest oscillation occurs near a channel width of 2. For very narrow channels, the particles are aligned in two parallel rows, but as the channel width is increased, it becomes energetically favorable for particles to be in the center of the channel so they leave the walls, thus increasing the wall spacing. As the channel width is further increased and the center of the channel is filled in with particles, it becomes less energetically favorable for the particles to be in the center of the channel and again the wall spacing decreases following approximately the 1D scaling. This process continues as the channel width is increased but the walls become farther removed from the center of the channel and therefore are less affected by the changes occurring there. Thus, the oscillations in the wall spacing decay after a channel width of ~ 5 where there is a buffer of at least one lattice line between the wall and the center of the channel. These oscillations are continuous as shown by the inset in Fig. 1(a), indicating that the addition of a new row in the center of the channel is a continuous process as the channel width is increased. The presence of these oscillations indicates that the channel width plays an important role in the types of structures that form in the 2D channel system. The oscillations in the wall spacing occur with a period $\sim R$ but the maxima and minima do not occur at integer multiples of R. This shows that the magic numbers are not simply integer multiples of R.

IV. LOW-TEMPERATURE-ANNEALED STRUCTURES

In order to study the properties of the crystal at a finite temperature, where thermal fluctuations become important, the 2D channel system was annealed to a temperature of $1/\Gamma = 0.062$ as in Sec. III. This temperature is in the solid phase for the unbounded 2D system.

A. Density profile

One measure that has been widely used to characterize the structure of a system confined between parallel planes is the equilibrium density profile of that system normal to the
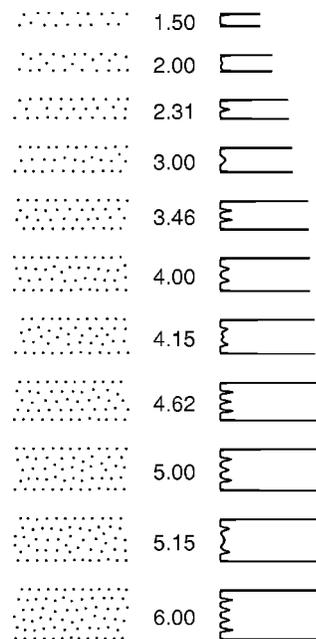
FIG. 2. Configuration snapshots, channel width, and equilibrium density profiles for selected dimensionless channel widths.

confining planes [20]. Figure 2 shows equilibrium density profiles transverse to the walls for a selection of channel widths. A characteristic feature of the density profiles is that they show a well-defined layered structure parallel to the walls similar to the aforementioned dusty plasma study [16]. This layered structure is evident even for channel widths of 100, implying that the system is in a solid state with rows that are parallel to the walls of the channel for all channel widths.

The sharpness of the peaks in the center of the channel varies nonmonotonically as the channel width is increased. The broadening and sharpening of the peaks always occurs near the center of the channel, showing that the layering near the walls is weakly affected by the increase in channel width, but the structure in the center of the channel undergoes large changes. The change in the structural properties in the center of the channel will prove important in characterizing the 2D dipole system in channels.

The most unique feature of the density profiles is the large peak in the profile occurring at each wall which was not observed in the dusty plasma study [16]. This peak is the result of the convolution of two collaborating effects. The increase in channel width causes an increase in the line density of the particles along the wall as seen in Fig. 1(a). Additionally, the long-ranged nature of the dipole-dipole interaction results in a net increase in the localization of the particles at the walls as the channel width is increased.

B. Transverse mobility at walls

The most direct measure of the transverse mobility of the particles localized at the wall is their mean-squared displacement (MSD) in the direction normal to the wall $\langle \Delta \tilde{x}^2(\tilde{\tau}) \rangle$ where $\tilde{\tau}$ is the dimensionless lag time. The wall particles are
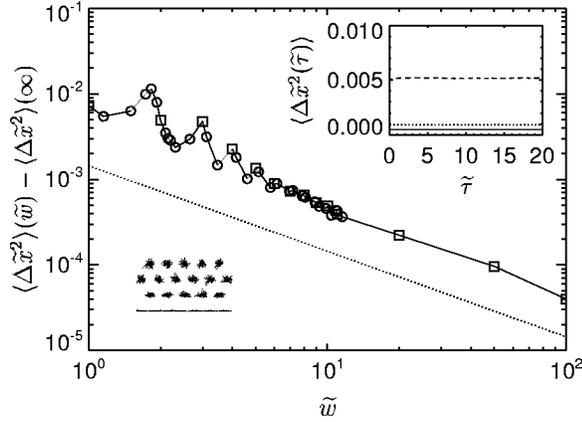
FIG. 3. Plateau value of the mean-squared displacement (MSD) of wall particles in the direction normal to the wall for selected dimensionless channel widths; square symbols correspond to integer channel widths and circle symbols correspond to noninteger channel widths. The value of $\langle\Delta\tilde{x}^2\rangle(\infty)$ is taken from an extrapolation of the simulation data. The dotted line is the approximation derived for the MSD [Eq. (19)] (without the constant term). Bottom left is a trace of the particle motion near the wall in a channel width of $\tilde{w}=10$, for a lag time of $\tilde{\tau}=3.73$, showing constrained motion at the wall. The top inset shows the MSD versus lag time for three channels: $\tilde{w}=3$ (dashed line), $\tilde{w}=10$ (dotted line), and $\tilde{w}=100$ (solid line).

defined as particles located within a distance $R/2$ from the wall. The MSD of the wall particles was observed to approach a plateau at long lag times (Fig. 3, inset), implying that the particles are localized at the wall for significant lengths of time. Eventually, the wall particles will migrate away from the wall but this was only rarely observed over the time scale of observation in Fig. 3. Additionally, this escape became increasingly unlikely as the channel width was increased. It was observed that the plateau value of the MSD decreases as the channel width is increased (Fig. 3), implying that the wall particles become more localized. This increased localization is a direct result of the long-ranged nature of the dipole interactions, combined with the presence of a hard wall, and contributes to the large peaks at the walls in the density profiles. In the limit of large channels, the MSD approaches a constant with a correction of order $\tilde{w}^{-1}$. This form for the MSD is expected when the potential near the walls is approximated by the sum of a near and a far contribution

$$\frac{V(\tilde{x},\tilde{w})}{k_BT} = \tilde{V}_{\text{near}}(\tilde{x},\tilde{w}) + \tilde{V}_{\text{far}}(\tilde{x},\tilde{w}). \tag{6}$$

The two parts of the potential are defined as

$$\tilde{V}_{\text{near}}(\tilde{x},\tilde{w}) = \Gamma R\rho_L \int_{-\infty}^{\infty} \frac{d\tilde{y}}{[(\tilde{c}-\tilde{x})^2+\tilde{y}^2]^{3/2}}, \tag{7}$$

$$\tilde{V}_{\text{far}}(\tilde{x},\tilde{w}) = \Gamma R^2 n \int_{2\tilde{c}}^{\tilde{w}} \int_{-\infty}^{\infty} \frac{d\tilde{y}dX}{[(X-\tilde{x})^2+\tilde{y}^2]^{3/2}}, \tag{8}$$

where $\tilde{c}$ is the x position of the first row away from the wall (the arbitrary cutoff between the near and far parts of the

potential) and ρ_L is the line density of the row. This definition of the potentials approximates the rows neighboring the walls as a continuum. This approximation introduces some error into the quantitative prediction for the MSD but does not affect the qualitative nature of the scaling. After the integrations, the potentials become

$$\tilde{V}_{\text{near}}(\tilde{x},\tilde{w}) = \frac{2\Gamma R\rho_L}{(\tilde{c}-\tilde{x})^2}, \tag{9}$$

$$\tilde{V}_{\text{far}}(\tilde{x},\tilde{w}) = 2\Gamma R^2 n\left(\frac{1}{2\tilde{c}-\tilde{x}} - \frac{1}{\tilde{w}-\tilde{x}}\right). \tag{10}$$

The dimensionless MSD in Fig. 3 is much smaller than one for all channel widths and, therefore, the potential can be expanded to first order near $\tilde{x}=0$ as

$$\tilde{V}(\tilde{x},\tilde{w}) \approx A(\tilde{w},\tilde{c}) + B(\tilde{w},\tilde{c})\tilde{x}, \tag{11}$$

where

$$A(\tilde{w},\tilde{c}) = \frac{2\Gamma R\rho_L}{\tilde{c}^2} + 2\Gamma R^2 n\left(\frac{1}{2\tilde{c}} - \frac{1}{\tilde{w}}\right), \tag{12}$$

$$B(\tilde{w},\tilde{c}) = \frac{4\Gamma R\rho_L}{\tilde{c}^3} + 2\Gamma R^2 n\left(\frac{1}{4\tilde{c}^2} - \frac{1}{\tilde{w}^2}\right). \tag{13}$$

The average MSD is given by the expression

$$\langle\Delta\tilde{x}^2\rangle(\tilde{w},\tilde{c}) = \langle(\tilde{x}(\tilde{\tau})-\tilde{x}(0))^2\rangle(\tilde{w},\tilde{c}). \tag{14}$$

In the long-time limit Eq. (14) can be written as

$$\lim_{\tilde{\tau}\to\infty}\langle\Delta\tilde{x}^2\rangle(\tilde{w},\tilde{c}) = 2\langle\tilde{x}^2\rangle(\tilde{w},\tilde{c}) - 2\langle\tilde{x}\rangle^2(\tilde{w},\tilde{c}). \tag{15}$$

This expression can be written as the integral

$$\lim_{\tilde{\tau}\to\infty}\langle\Delta\tilde{x}^2\rangle(\tilde{w},\tilde{c}) = 2\frac{\int_0^\varepsilon \tilde{x}^2 e^{-A-B\tilde{x}}d\tilde{x}}{\int_0^\varepsilon e^{-A-B\tilde{x}}d\tilde{x}} - 2\left(\frac{\int_0^\varepsilon \tilde{x}e^{-A-B\tilde{x}}d\tilde{x}}{\int_0^\varepsilon e^{-A-B\tilde{x}}d\tilde{x}}\right)^2. \tag{16}$$

Since the Boltzmann weighting goes to zero quickly as $\tilde{x}$ increases, the limit (ε) of the integration can be taken to infinity. The average MSD displacement then becomes

$$\lim_{\tilde{\tau}\to\infty}\langle\Delta\tilde{x}^2\rangle(\tilde{w},\tilde{c}) = \frac{4}{B^2} - \frac{2}{B^2} = \frac{2}{B^2}. \tag{17}$$

From the density profiles in Fig. 2 the position of the first peak away from the wall ($\tilde{c}$) can be calculated as a function of the channel width. This dependence is shown in Fig. 4 and is found to be

$$\tilde{c} \approx 1.0 + \frac{1.0}{\tilde{w}}. \tag{18}$$

Equation (18) implies that the separation between the row at the wall and the next row away is approximately equal to the lattice-line spacing in the unbounded 2D crystal (R) which is
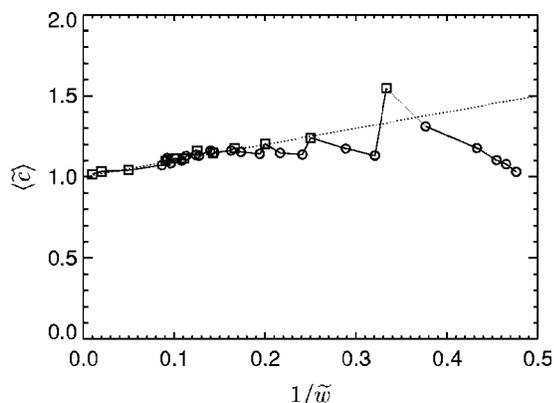
FIG. 4. x position of the first peak in the density profile for selected channel widths; square symbols correspond to integer channel widths and circle symbols correspond to noninteger channel widths. The dotted line is a linearfit to the data showing the functional form of $\tilde{c}$ in the limit of large $\tilde{w}$.

an intuitive result. The functional form of $\tilde{c}$ is important in determining how the MSD behaves as a function of the channel width. Combining Eqs. (13), (17), and (18) and expanding in the limit of large $\tilde{w}$ gives the approximate form for the average MSD as

$$\lim_{\tilde{\tau}\to\infty}\langle\Delta\tilde{x}^2\rangle(\tilde{w},\tilde{c}) \approx \frac{8}{\Gamma^2 R^2(Rn+8\rho_L)^2}\left(1+\frac{Rn+12\rho_L}{Rn+8\rho_L}\frac{1}{\tilde{w}}\right).$$

(19)

The result of this analysis is plotted as a dotted line in Fig. 3 (without the constant term) and is seen to predict the correct scaling behavior. The quantitative error in the prefactors is introduced by the many approximations made during the derivation of the MSD dependence on $\tilde{w}$. Importantly, the derivation of the MSD dependence shows that the interactions of the wall particles with the particles in their immediate vicinity (the neighboring row) are the dominant factor in determining the behavior of the MSD as a function of the channel width. The interactions with the particles farther away give higher-order corrections to the MSD scaling.

The data in Fig. 3 also show oscillations in the MSD as a function of the channel width. As in the case of the wall spacing [Fig. 1(a)] the oscillations decay after a channel width of ~ 5. This implies that effects of the changes occurring in the center of the channel are being shielded from the wall particles. There is a regular periodicity of the oscillations which is $\sim R$, implying that there are magic-number channel widths and in this case the maxima in the MSD data occur at integer multiples of R for channel widths greater than 2.

Figure 5 shows the physical changes occurring in the structure that give rise to the first oscillation. For channel widths less than ~ 2 there are two rows of particles, one on each wall. As the channel width is increased, the two rows of particles have weaker interactions, leading to an increase in the MSD plateau of the wall particles. Near a channel width of 2, particles begin to occupy the center of the channel. The
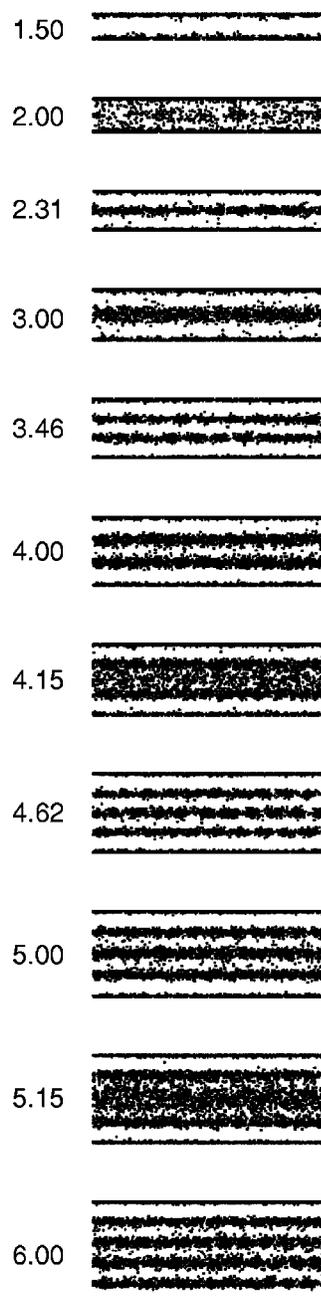
FIG. 5. Density of particles for selected dimensionless channel widths ($\tilde{w}=1.50-6.00$) for a total time of $\tilde{\tau}=37.3$ showing the oscillations between a loose and tight center row as the channel width is increased. Each point represents the position of a particle and points were drawn every $\tilde{\tau}=0.373$.

increased number of particles occupying the center of the channel results in a decrease of the MSD of the wall particles. For a channel width of 2.31 there is a well-defined row in the center of the channel, forcing the wall particles to remain near the wall, thus causing a minimum in the MSD at the wall. As the channel width is further increased, the center row begins to divide into two rows, causing a very loose structure to exist in the center of the channel. This loose structure allows the particles at the wall to fluctuate away more easily, resulting in a maximum for the MSD at a chan-

nel width of 3. Above a channel width of 3, the rows in the center of the channel begin to form and become distinct and at a channel width of 3.46 there are two distinct rows in the bulk, both of which force their respective neighboring wall particles to remain near the wall. A similar process is repeated as the channel width is increased from 3.46 to 4 (max MSD) to 4.62 (min MSD). The intermediate channel width of 4.15 shows a large amount of disorder in the bulk, so it is surprising that a maximum in the MSD does not occur at this channel width. However, in this channel, the first rows in the bulk remained well defined and therefore do not allow the wall particles to fluctuate away from the walls. At a channel width of 5 the row in the center of the channel again begins to broaden and the MSD at the walls passes through a maximum. However, in this case, the first row in from the wall is left relatively unchanged by this process and therefore the oscillations in the MSD of the wall particles are diminished for channel widths greater than 5. In Fig. 5 this effect is further illustrated by the channel widths of 4.15 and 5.15 where it is evident that there is disorder in the center of the channel but the first rows in the bulk remain well defined.

C. Structure analysis

The analysis of the density profiles and the MSD at the walls leads to the observation that the structural changes that take place in the crystal as the channel width is increased are occurring predominantly in the bulk for large channels. The structural changes in the bulk in turn affect the properties of the wall particles. In order to further understand the effect of channel width on the structure of the 2D crystal, it is necessary to measure the properties of the whole crystal, not just the properties at the walls. One measure of the structure of a 2D crystal is the defect concentration. For an unbounded system of dipoles in 2D the structure is purely hexagonal with each particle having six neighbors. Defect sites in that crystal are defined as sites which have more or less than the usual six neighbors. For wall particles in a channel, a defect is defined as a particle that would have more or less than six neighbors if the wall were not present. This translates to defects at the wall being defined as particles with more or less than four neighbors since a wall particle with four neighbors is equivalent to a nondefect site in the unbounded 2D case. This can be seen in the Delaunay triangle diagram in Fig. 1(b) where the crystal is triangular and each wall particle has four neighbors. For the nonwall particles (bulk particles) in the channel system, defects are defined in the same way as they are in the unbounded 2D crystal. The concentration of defect sites can be used to determine the state of the system [30,31], but here we are interested in using the defect concentration as a measure of how the channel system differs from the unbounded system.

The defect concentration as a function of channel width is shown in Fig. 6(a). Surprisingly, the defect concentration increases as the channel width is decreased. This is counterintuitive because the channel geometry is shown to stabilize layered structure near the walls as shown in the density profiles (Fig. 2). These two observations are reconciled by
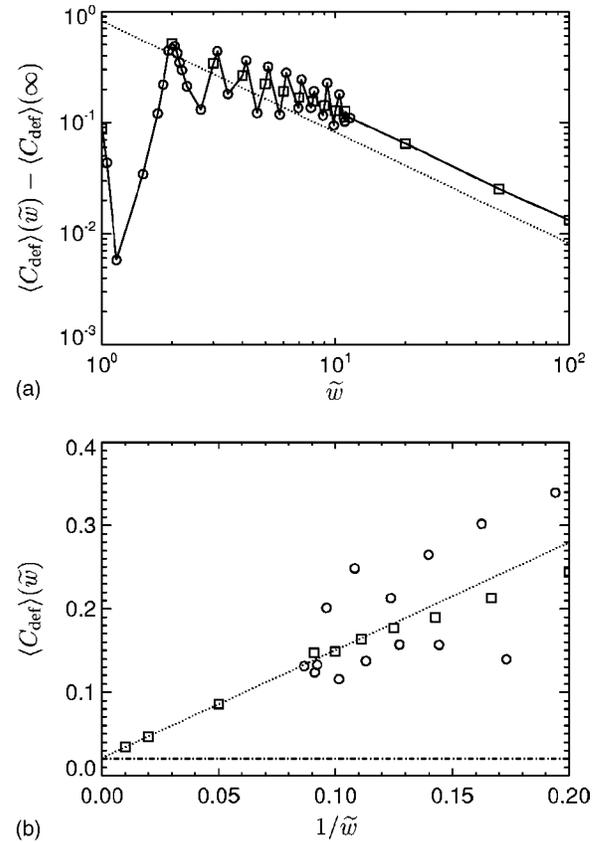
FIG. 6. (a) Defect concentration for selected dimensionless channel widths; square symbols correspond to integer channel widths and circle symbols correspond to noninteger channel widths. The dotted line is the prediction given by Eq. (24) (without the constant term). (b) The defect concentration approaches a constant as the channel width increases. The dash-dotted line corresponds to the equilibrium defect concentration in the unbounded system at a temperature of $1/\Gamma=0.062$.

noting that although the channel walls do impart a very nice layered structure near the walls, that structure is not perfectly hexagonal because the line density of the particles at the wall differs from that in the adjacent row. Therefore, the wall spacing is not commensurate with the bulk crystal spacing and as a result defects occur near the walls. For the narrow channels, the wall particles comprise a large portion of the system and therefore their higher defect concentration dominates the overall defect concentration of the system.

The behavior of the defect concentration as a function of the channel width in Fig. 6(a) is predicted by a simple argument. The concentration of defects is given by a bulk contribution and a wall contribution:

$$C_{def}(\widetilde{w}) = \frac{N_{def}}{N} = \frac{N_{def}^{b}}{N^{b}}\frac{N^{b}}{N} + \frac{N_{def}^{w}}{N^{w}}\frac{N^{w}}{N}, \qquad (20)$$

where N and N_{def} are the total number of particles and defects in the system, respectively. The parameters N^{b} and N^{w}
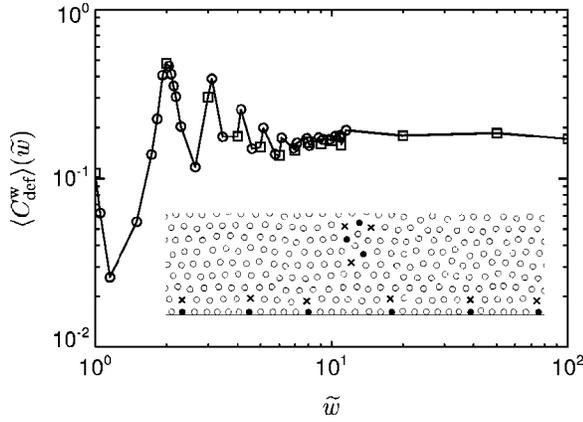
FIG. 7. Defect concentration at the wall for selected dimensionless channel widths; square symbols correspond to integer channel widths and circle symbols correspond to noninteger channel widths. The inset is a snapshot near the wall for a dimensionless channel width of 50 showing coordination of nearest neighbors; open thin circles correspond to sixfold-coordinated particles (or fourfold if on a wall), solid circles correspond to fivefold-coordinated particles (or threefold if on a wall), and $\times$ symbols correspond to sevenfold-coordinated particles (or fivefold if on a wall).

are the number of bulk and wall particles, respectively. Again, the boundary between the bulk region and the wall region is defined as a distance $R/2$ away from the walls. The ratios $N_{\text{def}}^{\text{b}}/N^{\text{b}}$ and $N_{\text{def}}^{\text{w}}/N^{\text{w}}$ can be approximated as constants equal to the unbounded system defect density and the semi-infinite wall-defect density, respectively. The wall-defect structure is shown in Fig. 7 (inset) where the defects along the walls are always accompanied by another defect in the first row of the bulk. Taking this into consideration, each wall defect in the semi-infinite limit actually induces another defect in the bulk and therefore the semi-infinite wall-defect density must be doubled. Therefore, the total defect concentration is approximated as

$$C_{\text{def}}(\widetilde{w}) \approx C_{\text{def}}^{\text{b}}(\infty)\frac{N^{\text{b}}}{N} + 2C_{\text{def}}^{\text{w}}(\infty)\frac{N^{\text{w}}}{N}. \quad (21)$$

Based upon the definition of the wall region, the two ratios in Eq. (21) can be approximated as

$$\frac{N^{\text{w}}}{N} \approx \frac{2\rho_{\text{w}}}{nw} = \frac{2R}{0.83w} = \frac{2}{0.83\widetilde{w}}, \quad (22)$$

$$\frac{N^{\text{b}}}{N} \approx 1 - \frac{2}{0.83\widetilde{w}}. \quad (23)$$

The parameter ρ_{w} is the line density along the wall and is equal to $(0.83a)^{-1}$ (from Sec. III) for large channels. The factor of 2 comes from the two walls. Therefore the total concentration of defects is approximated as

$$C_{\text{def}}(\widetilde{w}) \approx C_{\text{def}}^{\text{b}}(\infty) + [2C_{\text{def}}^{\text{w}}(\infty) - C_{\text{def}}^{\text{b}}(\infty)]\frac{2}{0.83\widetilde{w}}, \quad (24)$$

in the limit of large channels. The values of $C_{\text{def}}^{\text{b}}(\infty)$ and $C_{\text{def}}^{\text{w}}(\infty)$ were obtained by extrapolating the simulation data in the channels. This approximation (constant plus correction of order $\widetilde{w}^{-1}$) is seen as a dotted line in Fig. 6(a) and additionally the total defect concentration is observed to approach the unbounded limit of 0.02 exactly as the channel width gets very large in Fig. 6(b). This observation implies that the defect properties of the channel system approach the unbounded system in the limit of large channels, as expected. Even for large channels, however, there is still a large concentration of defects at the walls as seen in Fig. 7. The concentration of wall defects goes to a constant in the limit of large channels. The value that the wall-defect density approaches (0.18) is much larger than the value that the bulk-defect density approaches (0.02). The cause of this higher defect density can be seen in Fig. 7 (inset) where there are stable dislocations along the length of the wall. In the unbounded system, a dislocation is defined as a pair of neighboring particles with five and seven neighbors, respectively. Along the wall in the channel system, a dislocation is defined as a wall particle with three or five neighbors neighboring a bulk particle with seven or five neighbors, respectively. Along the wall, 18% of the total wall particles are part of a dislocation and are the cause of the higher density of defects at the wall. The dislocations along the walls are spaced evenly, which is a consequence of the differing line densities along the wall and in the first row. The different line densities force wall particles and their neighboring row to form dislocations at regular intervals in order to minimize the energy of interaction between these two rows.

The oscillations in defect concentration as a function of channel width decay much more slowly than the oscillations in the wall spacing or MSD. The splitting of the center row into two rows as the channel width is increased causes a loose structure to form in the center of the channel and increases the defect concentration in the channel. When there are well-defined rows in the center of the channel, the structure there is very regular and therefore the defect concentration in the channel is lower. As in the case of the wall spacing and the MSD, the periodicity of the oscillations in the defect density is $\sim R$ but in this case the maxima and minima do not occur at integer multiples of R. The oscillations in defect density persist for large channels ($\widetilde{w} > 10$), indicating that the structure in the center of wide channels is still strongly influenced by the channel width. At the walls, however, the oscillations in the wall-defect concentration decay by a channel with of ~ 5. The combination of these two observations leads to the conclusion that the long-lived oscillations in total defect concentration are due to bulk contributions and not the walls. Therefore, the structural changes due to changing channel width are predominantly manifested in the center of the channel and the structure near the walls is influenced in a secondary manner. The long-lived nature of the oscillations indicates that defect concentration is a very
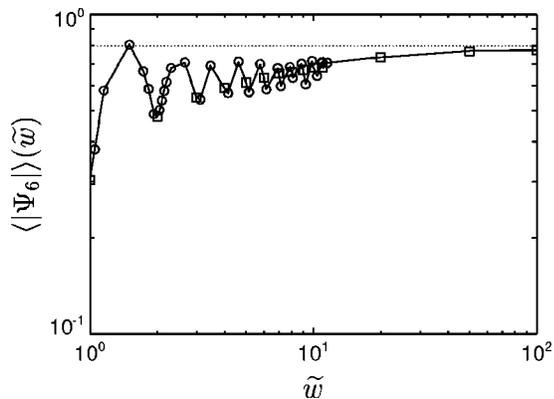
FIG. 8. Average local bond-orientation order for selected channel widths; square symbols correspond to integer channel widths and circle symbols correspond to noninteger channel widths. The dotted line corresponds to the value of $\langle|\Psi_6|\rangle$ for an unbounded system at a temperature of $1/\Gamma = 0.062$.

sensitive measure of the effects of channel width on the crystal structure in the channel.

Another factor indicating the nature of the structure of the 2D crystal is the average local bond-orientation order $\langle|\Psi_6|\rangle$. This parameter is a measure of the angles between a particle and its nearest neighbors. It is defined as

$$\langle|\Psi_6|\rangle = \frac{1}{N}\sum^{N}\left|\frac{1}{m}\sum_{k=1}^{m} e^{i6\theta_k}\right|, \qquad (25)$$

where m is the number of neighbors for a given particle and θ_k is the angle between the vector connecting the particle and its kth nearest neighbor and an arbitrary reference axis. When the lattice is perfectly hexagonal, $\langle|\Psi_6|\rangle = 1$. Additionally, if the lattice is six fold coordinated and has few defects, it can still be deformed by the presence of the walls [as shown by the Delaunay triangles in Fig. 1(b)], causing $\langle|\Psi_6|\rangle$ to deviate from a value of 1. The average local bond-orientation order is shown in Fig. 8 as a function of channel width. For very narrow channels $\tilde{w} < 2$, there are large oscillations in $\langle|\Psi_6|\rangle$ due to the structure switching back and forth as the channel width is increased from a nicely hexagonal lattice to a triangular lattice with angles that deviate from 60°. The average value of $|\Psi_6|$ approaches the value for the unbounded system with a correction $\tilde{w}^{-1}$. For channel widths greater than 2, the oscillations in $\langle|\Psi_6|\rangle$ are well correlated with those for the defect concentration. This correlation indicates that the oscillations in $\langle|\Psi_6|\rangle$ are due to defects and not to the deformation of the angles in a triangular lattice from the normal 60°.

V. SUMMARY

A structural analysis has been performed on a system of particles interacting with a purely repulsive dipolar interaction confined in 2D channels. The application of parallel planar walls to the system of 2D dipoles results in unique and sometimes surprising structural properties. This system has not been explored in the literature and it is important in further understanding the effects of confinement on colloidal systems. The alignment of the crystal in the direction of the walls is expected for any confined colloidal system; however, the large magnitude of the wall peaks in the density profile is a unique property of the long-ranged nature of the particle interactions. The spreading of the peaks in the center of the channel, for channel widths not commensurate with the natural crystal, indicates a loss of structure in that region. The defect concentration and local bond-orientational order in the channel confirm that the local structure is disrupted in these channels. The oscillations in all of the structural properties indicate that the structure of the crystal in the 2D channel system can be altered by slight changes in the channel width. This is a very important observation for any application that is highly dependent on the type of structure in the channel. Additionally, the slow approach ($\tilde{w}^{-1}$) of the system properties to their unbounded values indicate that channel-like confinement, even fairly large channels, drastically changes the structural properties of the 2D dipolar crystal.

The structural analysis of the dipole system in 2D channels shows many similarities to other studies of confined 2D systems. Wall-induced layering is observed in this system analogous to the layering observed in a dusty-plasma study [16] and the shell structure in circular confinements [10–14]. However, in the case of repulsive magnetic dipoles there is a higher density and localization at the walls in the 2D channel system than in the dustyplasma system. The increased density is the cause of the unique structural properties that occur in the 2D crystal near the wall, such as evenly spaced stable dislocations. Extreme localization of the wall particles has been observed in hard circular confinement studies with long-ranged repulsive interactions [10]. However, the increased localization as a function of the channel width is an important observation in this study in that it shows how the addition of walls continues to influence the behavior of the system, even for large channel widths. Similar to the dusty-plasma study, order-disorder transitions were observed in the channel by observing the alternate sharpening and broadening of the density peaks as the channel width was increased. However, in the case of the dipole interactions, the wall peak actually increases in magnitude as the channel width is increased due to the long-ranged nature of the interparticle interactions and the presence of the hard wall. Also, the sharpening and broadening of the peaks only occurs near the center of the channel in the case of dipolar interactions, indicating that the structure of the crystal in the center of the channel changes significantly with only slight changes in the channel width. The oscillations in the structural properties as a function of the channel width occur with a regular period $\sim R$, indicating that there are certain regular intervals of channel widths, magic numbers, that are commensurate with the natural structure of dipolar particles in 2D channels. These magic numbers do not occur at integer multiples of R, as expected, but are influenced by such system properties as the high density at the walls. This observation is important in that it indicates that there is an appropriate, yet complex, methodology for predicting the structures that will form in the channel system.

Other studies on the structure and dynamics of 2D dipole systems under confinement have shown that the nature of the melting transition is altered due to the confinement [10–12,14]. The structural properties of these confined systems have a strong influence on the nature of the phase transition—where it begins and how it proceeds. In the case of 2D channels we have observed structural properties of the crystal which, in the context of previous studies [10–14], will likely prove important in studying the phase transition in the 2D channel system. These other interesting properties of the 2D channel system will be discussed in future work. The study presented here serves as an introduction to the funda-mental structural properties of self-assembled dipole systems in 2D channel geometries.

[1] P. S. Doyle, J. Bibette, A. Bancaud, and J.-L. Viovy, Science **295**, 2237 (2002).

[2] Y. S. Lee, E. Wetzel, and N. Wagner, J. Mater. Sci. **38**, 2825 (2003).

[3] H. Löwen, Phys. Rev. E **53**, R29 (1996).

[4] K. Zahn, R. Lenke, and G. Maret, Phys. Rev. Lett. **82**, 2721 (1999).

[5] K. Zahn and G. Maret, Phys. Rev. Lett. **85**, 3656 (2000).

[6] R. Pesché, M. Kollmann, and G. Nägele, Phys. Rev. E **64**, 052401 (2001).

[7] J. Kosterlitz and J. Thouless, J. Phys. C **6**, 1181 (1973).

[8] B. I. Halperin and D. R. Nelson, Phys. Rev. Lett. **41**, 121 (1978).

[9] A. P. Young, Phys. Rev. B **19**, 1855 (1979).

[10] V. M. Bedanov and F. M. Peeters, Phys. Rev. B **49**, 2667 (1994).

[11] R. Bubeck, C. Bechinger, S. Neser, and P. Leiderer, Phys. Rev. Lett. **82**, 3364 (1999).

[12] Y.-J. Lai and L. I, Phys. Rev. E **64**, 015601 (2001).

[13] R. Bubeck, P. Leiderer, and C. Bechinger, Europhys. Lett. **60**, 474 (2002).

[14] M. Kong, B. Partoens, and F. M. Peeters, Phys. Rev. E **67**, 021608 (2003).

[15] C. Bechinger, M. Brunner, and P. Leiderer, Phys. Rev. Lett. **86**, 930 (2001).

[16] L.-W. Teng, P.-S. Tu, and L. I, Phys. Rev. Lett. **90**, 245004 (2003).

[17] R. A. Segalman, A. Hexemer, and E. J. Kramer, Macromolecules **36**, 6831 (2003).

[18] R. A. Segalman, A. Hexemer, and E. J. Kramer, Phys. Rev. Lett. **91**, 196101 (2003).

[19] B. Bhushan, J. N. Israelachvili, and U. Landman, Nature (London) **374**, 607 (1995).

[20] J. Gao, W. D. Luedtke, and U. Landman, Phys. Rev. Lett. **79**, 705 (1997).

[21] E. M. Lawrence, M. L. Ivey, G. A. Flores, J. Liu, J. Bibette, and J. Richard, Int. J. Mod. Phys. B **8**, 2765 (1994).

[22] K. Zahn, J. Méndez-Alcaraz, and G. Maret, Phys. Rev. Lett. **79**, 175 (1997).

[23] H. Zhang and M. Widom, Phys. Rev. E **51**, 2099 (1995).

[24] R. Kalia and P. Vashishta, J. Phys. C **14**, L643 (1981).

[25] B. Rinn, K. Zahn, P. Maass, and G. Maret, Europhys. Lett. **46**, 537 (1999).

[26] H. C. Öttinger, *Stochastic Processes in Polymeric Fluids: Tools and Examples for Developing Simulation Algorithms* (Springer, Berlin, 1996).

[27] D. Heyes and J. Melrose, J. Non-Newtonian Fluid Mech. **46**, 1 (1993).

[28] D. Frenkel and B. Smit, *Understanding Molecular Simulation from Algorithms to Applications*, 2nd ed. (MPG, Bodmin, Great Britain, 2002).

[29] K. J. Strandburg, Rev. Mod. Phys. **60**, 161 (1988).

[30] J. Q. Broughton, G. H. Gilmer, and J. D. Weeks, Phys. Rev. B **25**, 4651 (1982).

[31] M. P. Allen, D. Frenkel, W. Gignac, and J. P. McTague, J. Chem. Phys. **78**, 4206 (1983).